Desalination and Water Treatment
www.deswater.com

doi: 10.5004/dwt.2023.30038

314 (2023) 330–338
December

Air gap fluid flow characteristics of high-power water-cooled submersible motors

Shibin Zhang[a,*], Huayang Ren[a], Dingtang Zhang[b], Shuai Wang[c,d], Huyi Zhang[e], Rui Luo[f], Yunbing Feng[g]

[a]*School of Mechanical Engineering, North China University of Water Resources and Electric Power, Zhengzhou 450000, China, Tel.: +86 17638191393; email: zhangyh886@163.com (S.B. Zhang)*
[b]*Zhengzhou Coal Mining Machinery (Group) Co., Ltd., Zhengzhou 450000, China*
[c]*College of Safety Science and Engineering, Liaoning Technical University, Fuxin 123000, China*
[d]*Fushun China Coal Technology Engineering Testing Center Co., Ltd., Fushun 113122, China*
[e]*School of Shanghai Maritime University, Shanghai 200135, China*
[f]*Hebi Vocational College of Energy and Chemistry, Hebi 458000, China*
[g]*Zhengzhou Coal Industry (Group) Co., Ltd., Zhengzhou 450000, China*

Received 19 November 2022; Accepted 13 September 2023

ABSTRACT

The rotor of a high-power water-filled submersible motor rotates at high speed in liquid during operation. while working motor internal air gap fluid flow in complicated cases, fluid flow characteristics is not only directly affect the water of the rotor friction loss, also affect the submersible motor cooling effect. In this paper, the fluid field in the inner cavity of submersible motor is deeply studied. The air-gap fluid grid model was established according to computational fluid dynamics, and the influence of air-gap on fluid velocity of submersible motor was studied based on ANSYS and FLUENT software. The results show that the pressure decreases linearly after the cooling water enters the motor air gap, the maximum pressure is located at the air gap inlet and the minimum at the air gap outlet; the outlet and inlet pressure of the air gap fluid grows with the increase of the air gap inlet fluid flow rate, and the growth rate tends to decrease in different degrees. The research results provide a basis for the design of submersible motor and the determination of the reasonable flow of fluid in the motor.

Keywords: Submersible motor; Fluid grid; Air gap; Flow characteristics

1. Introduction

Among the submersible motor faults that occur during the operation of high-powered submersible motors, the most common failure is due to overheating inside the submersible motor or excessive local temperature rise leading to motor winding or lead insulation failure [1–3], and the flow characteristics of the cooling medium inside the submersible motor directly affect the cooling effect of the motor [4]. Therefore, the study of the temperature field of the submersible motor inevitably requires the study of the flow characteristics of its internal cooling [5].

So far, some scholars and experts have generally focused on the structural performance of the motor, the internal temperature rise distribution and the fluid flow characteristics of the motor. Zhao and Luo [6] use analytical method to analyze the causes of noise vibration and abnormal noise of permanent magnet synchronous motor, and verifies the simulation by manufacturing a prototype. Zhang et al. [7] established two temperature field

* Corresponding author.

models by using the finite volume method (FVM), pointed out the importance of oil friction loss and copper loss as variables, proposed the design process of the cooling system, and obtained the design range between the structural parameters of the radiator and the circulation flow. Zheng et al. [8] studied the law of turbulent flow in a water-filled submersible motor based on the three-dimensional numerical simulation method of ANSYS-CFD software. Guan et al. [9] proposed a numerical model based on the eccentricity analysis method to simulate the bearing failure process of submersible induction motor. The effects of rotor deflection on air gap magnetic density and field electromagnetic force are analyzed by using two-dimensional Fourier decomposition method. According to the structural characteristics of the submersible motor, Xu et al. [10] studied the influence of the segmental characteristics of fixed rotor on the design and performance of submersible motor, and improved the measuring method of submersible motor.

Some experts have focused on different motors such as permanent magnet synchronous motors [11], hydroelectric generators, and turbine generators, opening up excellent and effective analytical studies on their fluid flow characteristics under the cooling structure and temperature rise distribution. The main methods used are finite element analysis [12], FVM [13], and thermal mesh method [14].

Wang et al. [15] proposed a new IPMSM based on the internal fan of the axial ventilation cooling structure, and improved the cooling structure of the motor by using computational fluid dynamics (CFD) to analyze the wind speed distribution and temperature distribution characteristics inside the motor. Shi et al. [16] put forward the control method and operation mode with Siemens PLC (Munich and Berlin, Germany) as the core, designed the air-cooled heat exchanger and the liquid-cooled radiator of the heat dissipation system, and optimized the cooling tube layout and pipeline layout of the air-cooled heat exchanger and the liquid-cooled radiator.

According to the available references, for high-power submersible motors, researchers generally focus on the fluid flow characteristics flow characteristics inside the motor under different cooling media, and most of the literature use the finite element method to calculate the model and establish the air gap fluid mesh model based on CFD principles to analyze the three-dimensional model of the air gap of high-power submersible motors [17,18]. However, the fluid flow rate in the air gap inlet and outlet affects the motor operating temperature and cooling condition, so it is meaningful to study the fluid flow in the air gap inside the submersible motor.

In this paper, 3,200 kW water-filled submersible motor is taken as the research object. Based on the finite element analysis method and Re-Normalisation Group (RNG) k–ε two-equation turbulence model, the air-gap fluid grid model of submersible motor is established by CFD, and the influence of rotor speed and air-gap inlet and outlet fluid velocity on the flow characteristics of water-filled submersible motor is studied. The results obtained by detailed research will provide a certain reference for the design of this kind of water-filled submersible motor and the determination of reasonable fluid flow in the motor.

2. Structure and parameters description

2.1. Cooling structure

High power submersible motors work for long hours in mines and have high ambient temperatures. The high-power submersible motor has long working time and high ambient temperature in the mine. It is necessary to fill with cooling water or lubricating oil to ensure the lubrication and heat dissipation between the parts inside the submersible motor, so the water circulation cooling structure is designed inside the motor. The overall structure of the water-filled submersible motor is shown in Fig. 1. The assembly model of submersible motor cooling structure is shown in Fig. 2.

2.2. Parameters of submersible motor

In order to better understand the structure of submersible motors, a 3,200 kW submersible motor is used as an example and its basic parameters are shown in Table 1.

3. Modeling for thermal analysis of the submersible motor

In order to study the flow characteristics of fluid in the air gap of the water filled submersible motor stator and rotor, the submersible motor flow field is modelled and simulated according to the available structural parameters.

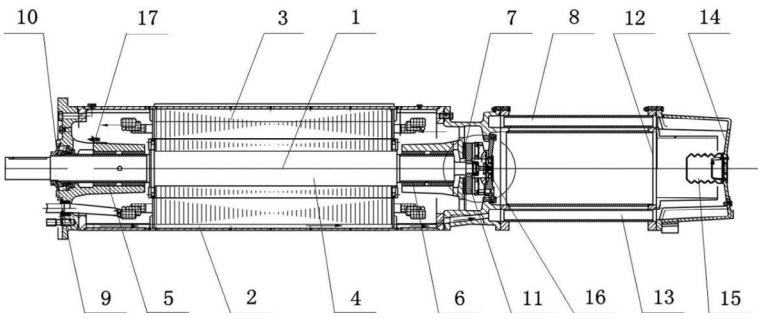

Fig. 1. Deep well water-filled submersible motor overall structure diagram. 1-Motor shaft; 2-Motor casing; 3-Stator assembly; 4-Rotor component; 5-Upper guide bearing; 6-Lower guide bearing; 7-Thrust bearing assembly; 8-Cooling radiator; 9-Mechanical sealing device; 10-Sand throwing ring; 11-Thrusting disc; 12-Filter; 13-Cooling water tank; 14-Base; 15-Adjustment capsule; 16-Drive pump wheel; 17-Poor water sensor.

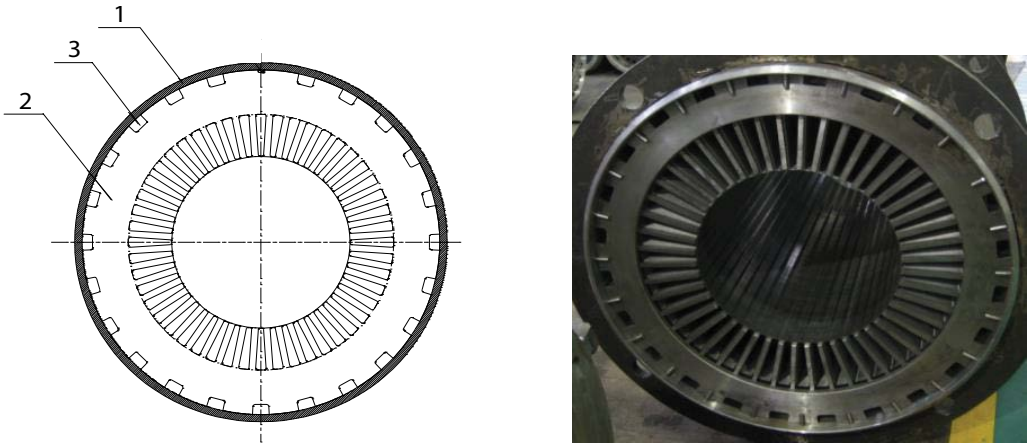

Fig. 2. Assembly model of submersible motor cooling structure. 1-Motor casing; 2-Stator component; 3-Cooling channel.

Table 1
Basic parameters about 3,200 kW water-filled submersible motor

Parameter	Value
Power	3,200 kW
Voltage	10 kV
Inner diameter of stator	423 mm
Outer diameter of rotor	417 mm
Supporting circulation pump wheel	Flow rate of 40 m^3/h, head range of 10 m
Air gap height	3 mm
Design temperature rise	When the ambient temperature is 40°C, the temperature rise shall not exceed 40°C

3.1. Basic assumptions of internal flow field analysis

Before solving the flow field and setting the boundary, the following reasonable assumptions are made for the simulation model from the perspective of fluid dynamics:

(1) Cooling water enters the motor stator and rotor air gap along the motor axis.
(2) Set the inlet air gap of the motor as the velocity boundary, the outlet air gap of the motor boundary as the pressure boundary, Set the outlet pressure to be equal to 1 atmospheric pressure.
(3) Set the intersection of air gap and stator and rotor as the motion boundary, the two sections of air gap along the motor axis are set as symmetric boundary, and rotor speed and rotor surface roughness are set in the rotor intersection.
(4) Air gap is an in-compressible fluid, the inlet temperature is set to 285 K, and the fluid density does not change during operation.

3.2. Governing equations

The flow characteristics inside the submersible motor are analysed using FLUENT for simulation solutions. The flow of fluid in the motor follows the conservation of mass and the conservation of momentum.

3.2.1. Mass conservation equation

The mass conservation equation of fluid in continuous flow can be expressed as:

$$\nabla\left(\rho V\right)+\frac{\partial\rho}{\partial\tau}=0 \tag{1}$$

where ρ represents fluid density; τ represents time; V represents the velocity; ∇ is a Hamilton operator.

3.2.2. Momentum conservation equation

In the process of fluid flow, conservation of momentum must be satisfied, the momentum conservation equation of a fluid in continuous flow can be expressed as:

$$\frac{\partial}{\partial\tau}\left(\rho v\right)+\nabla\cdot\rho v\cdot v=F-\nabla p+\nabla\left(F_{\tau}\right) \tag{2}$$

where p represents the pressure of the fluid; F represents unit volume force; v is the viscous force tensor.

3.3. Mathematical model

The standard RNG k–ε two-path turbulence model is selected for calculation. The model has good applicability

to curved flow lines such as rotating flow with large centrifugal force, and the model equation can be expressed as:

$$\frac{\partial}{\partial t}(\rho k)+\frac{\partial}{\partial x_i}(\rho u,k)=\frac{\partial}{\partial x_j}\left(\alpha_k\mu_{\text{eff}}\frac{\partial k}{\partial x_j}\right)+G_k+\rho\varepsilon \quad (3)$$

$$\frac{\partial}{\partial t}(\rho\varepsilon)+\frac{\partial}{\partial x_i}(\rho u_i\varepsilon)=\frac{\partial}{\partial x_j}\left(\alpha_\varepsilon\mu_{\text{eff}}\frac{\partial\varepsilon}{\partial x_j}\right)+\frac{C_{1\varepsilon}\times\varepsilon}{k}G_k-C_{2\varepsilon}\rho\frac{\varepsilon^2}{k} \quad (4)$$

where $\mu_{\text{eff}} = \mu + \mu_t$ correction coefficient.

The shift of the fluid mesh is controlled by the dynamic mesh UDF program to effectively correct the offset angle. For constant, incompressible fluids, the constant pressure solver is used, and the SIMPLE algorithm is chosen for the coupled pressure-velocity solution.

3.4. Mesh generation

Fluent software is used to establish the air-gap fluid model of submersible motor. The quality of mesh is directly related to the accuracy of numerical calculation results. Air gap fluid belongs to annular structure, which requires high precision. The height of the air gap is smaller than the overall size of the motor, so the quality of the boundary layer grid needs to be controlled. Meet the operation requirements of GAMBIT software; GAMBIT software is used for structured mesh division, which can ignore the convex and concave structures on the outer surface of the rotor and the inner surface of the stator. Hexahedral mesh cells were used to divide 709,389 units and generate 795,000 nodes. The minimum volume mesh cells were positive. The mesh irrelevance check proves that the mesh quality is good and can be used directly for fluid simulation analysis, meeting the computational requirements of FLUENT. The meshing effect is shown in Fig. 3.

In order to reduce the calculation time while ensuring accurate analysis results. The water-filled submersible motor air gap fluid grid model can be partitioned according to the symmetric boundary conditions, taking the submersible motor air gap fluid 1/4-mesh model for simulation and setting the tangent surface as a symmetric boundary, and the model is shown in Fig. 4.

4. Numerical analysis of fluid field

The hypothesis and the fluid field model that the fluid flow at the inlet of the air gap affects the fluid flow and fluid pressure in the air gap during the operation of submersible motor are simulated and analyzed.

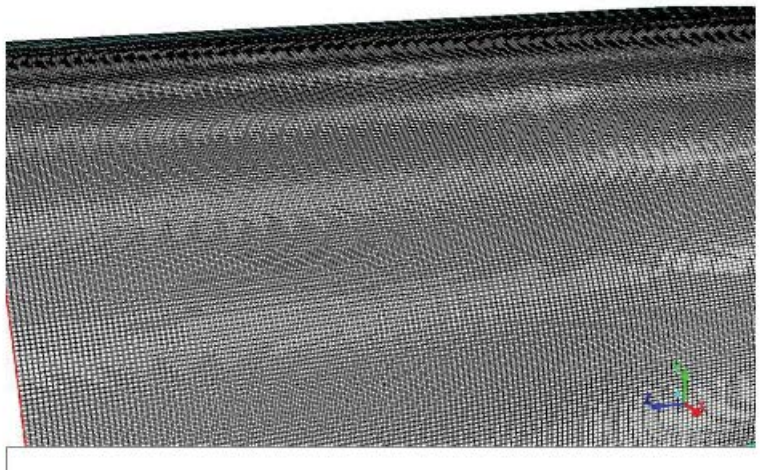

Fig. 3. Fluid meshing effect of motor air gap.

Fig. 4. Motor air gap fluid 1/4 model.

4.1. Effect of air gap inlet fluid flow rate on fluid flow rate

Fig. 5a–d show the internal velocity distribution clouds of the fluid in the air gap of the motor when the flow velocity is 1, 2, 3 and 4 m/s, respectively. In order to study the influence of air gap inlet fluid velocity on the flow velocity distribution of motor air gap fluid, a cross section parallel to the XY plane is taken at a suitable position along the stator axial direction (*Z*-axis direction) in each velocity cloud, and the velocity cloud shows that the velocity changes quickly at the air gap inlet, the cross section interval is taken to be smaller, and the velocity at the back end of the air gap is relatively stable, the cross section interval is taken to be larger. Calculate the average velocity of the cross-sectional fluid, and display the average velocity of the fluid in the cross-section in 2D and 3D coordinate systems. Air gap fluid velocity distribution cloud are shown in Fig. 6.

Analysis of Figs. 5 and 6 can lead to the following conclusions: after the fluid in the motor enters the motor air gap, the velocity of the fluid increases rapidly when the submersible motor rotor rotates at high speed, and then

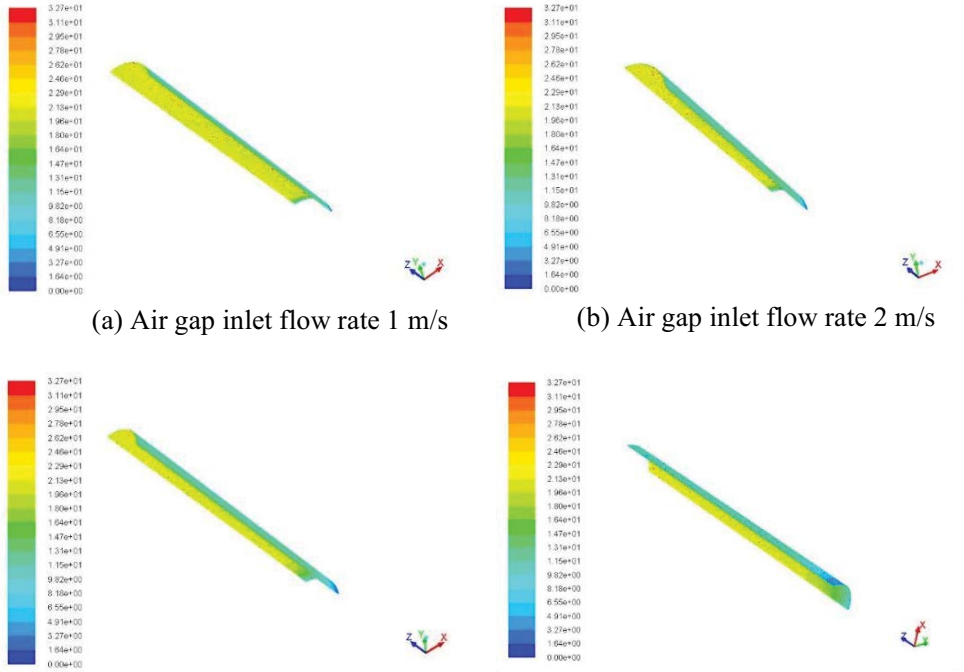

(a) Air gap inlet flow rate 1 m/s (b) Air gap inlet flow rate 2 m/s

(c) Air gap inlet flow rate 3 m/s (d) Air gap inlet flow rate 4 m/s

Fig. 5. Air gap fluid velocity distribution cloud. Air gap inlet flow rate (a) 1 m/s, (b) 2 m/s, (c) 3 m/s, and (d) 4 m/s.

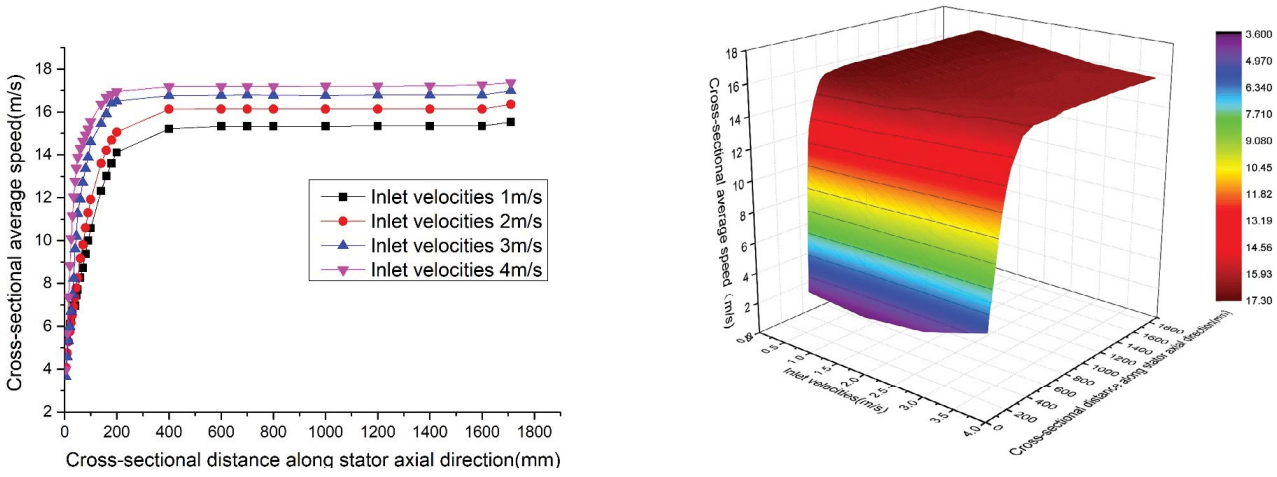

(a) **(b)**

Fig. 6. Average velocity distribution of air gap fluid at different inlet speeds.

the fluid velocity quickly reaches a relatively stable state. In this process, the maximum velocity is located at the side wall of the motor rotor, the minimum velocity is located at the inner wall of the motor stator, and the minimum velocity value is 0. The steady state average velocity of air gap fluid corresponding to 1, 2, 3 and 4 m/s are 15.33, 16.13, 16.78 and 17.19 m/s, through analysis, it can be concluded that the average value of air gap fluid flow rate increases with the increase of air gap inlet flow rate, and the growth rate gradually decreases. The effect of different inlet velocities on the stable average flow velocity of air gap fluid is shown in Fig. 7.

4.2. Effect of air gap inlet fluid flow rate on fluid pressure

Fig. 8a–d show the fluid pressure distribution clouds inside the submersible motor air gap when the gap inlet fluid velocity is 1, 2, 3 and 4 m/s, the colored strips shown in Fig. 8 are the pressure contours. In order to understand more intuitively the effect of air gap inlet fluid flow velocity on the pressure distribution in the submersible motor air gap, 16 equally spaced cross sections parallel to the XY plane are taken at equal distances along the stator axial direction (Z-axis direction) in each pressure cloud, and the average pressure value of the fluid in the cross sections is calculated, and then the average pressure of the fluid in the cross sections is displayed in the two-dimensional and three-dimensional coordinate system. The average pressure distribution of air gap fluid at different inlet speeds is shown in Fig. 9.

Analysis of Figs. 8 and 9 can be concluded as follows: after the fluid inside the motor enters the stator and rotor air gap, the pressure contour is irregular, indicating that the internal fluid is in a turbulent state. Fig. 9a shows the average value of the cross-sectional pressure is linearly decreasing along the motor axial direction, the maximum pressure value of the submersible motor air gap is the gap inlet, the minimum value is at the air gap outlet, which is equal to the ambient pressure. The inlet pressure corresponding to the air gap inlet fluid axial velocity of 1, 2, 3 and 4 m/s are 1.0416, 1.0828, 1.1201 and 1.1512 MPa, respectively, and the outlet pressure is 1.0 MPa, and the pressure drops of import and export are 0.0416, 0.0828, 0.1201, 0.1512 and 0.1512 MPa. The pressure drop at the inlet and outlet of the motor air gap fluid increases and returns with the increase of the air gap fluid flow rate, as shown in Fig. 10.

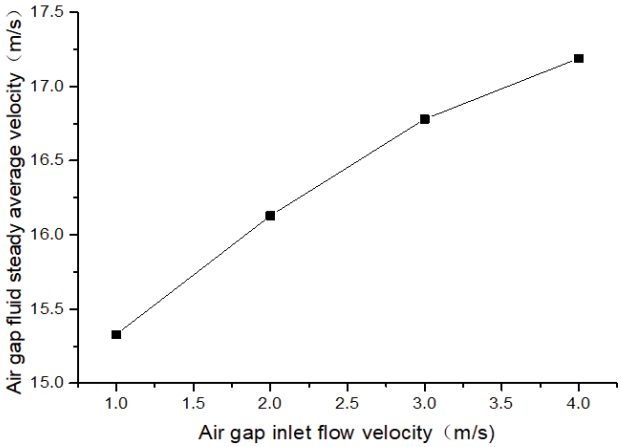

Fig. 7. Effect of different inlet velocities on the stable average flow velocity of air gap fluid.

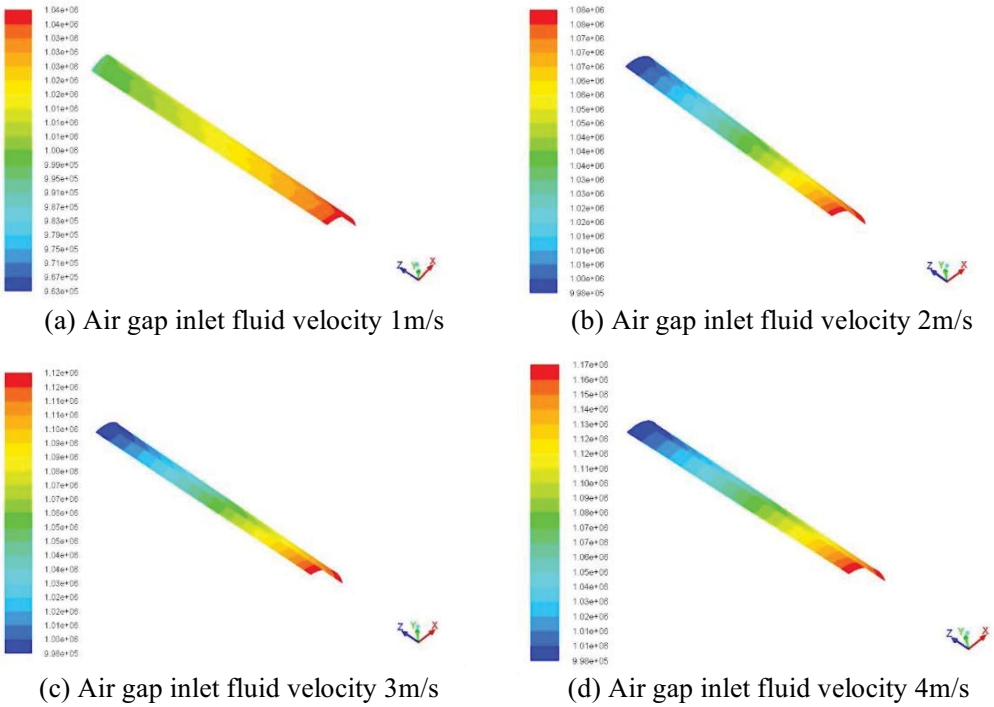

(a) Air gap inlet fluid velocity 1m/s (b) Air gap inlet fluid velocity 2m/s

(c) Air gap inlet fluid velocity 3m/s (d) Air gap inlet fluid velocity 4m/s

Fig. 8. Air gap fluid pressure distribution cloud. Air gap inlet fluid velocity (a) 1 m/s, (b) 2 m/s, (c) 3 m/s and (d) 4 m/s.

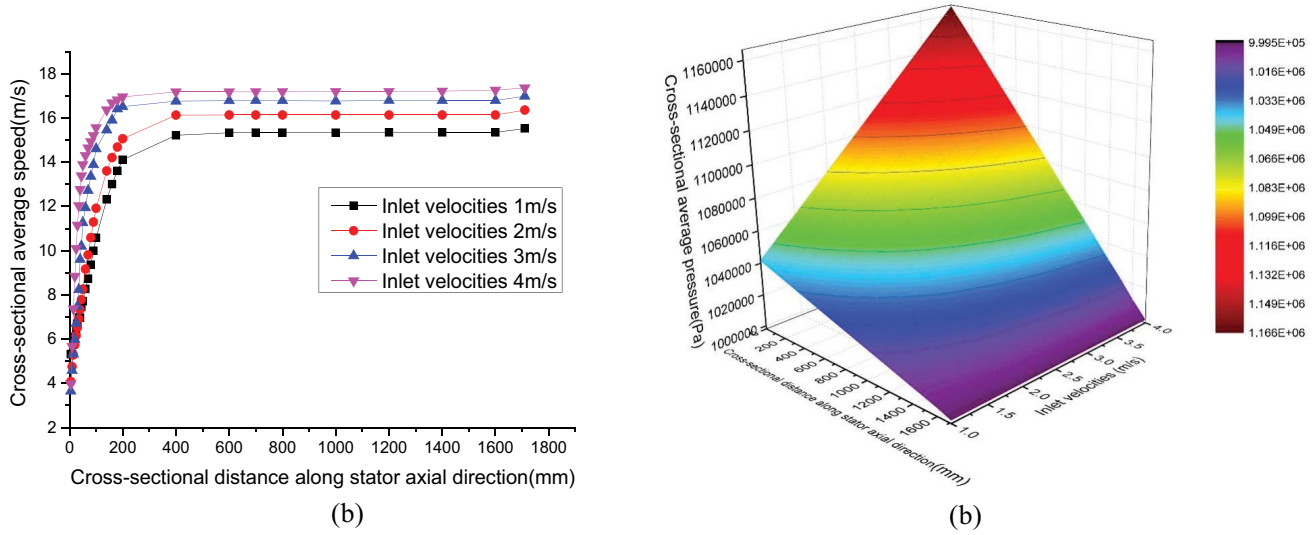

Fig. 9. Average pressure distribution of air gap fluid at different inlet speeds.

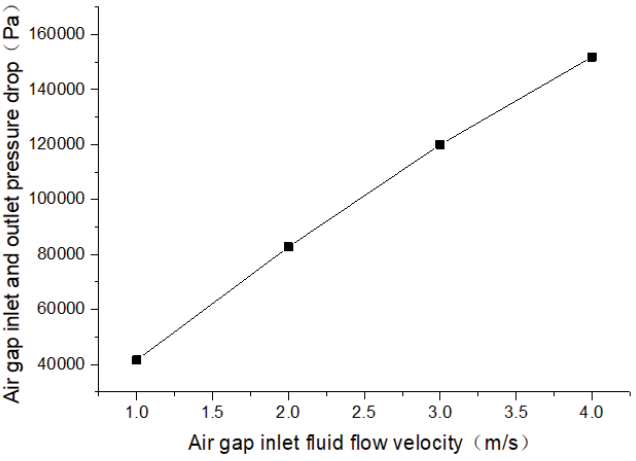

Fig. 10. Air gap fluid pressure drop with the change of the air flow rate of fluid inlet.

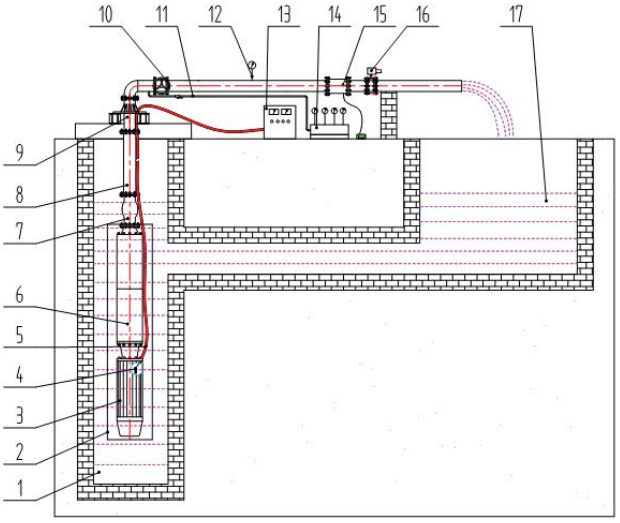

Fig. 11. Deep well submersible pump comprehensive test platform schematic. 1-Experimental well; 2-Suction chamber; 3-Wet submersible motor; 4-Pressure sensor; 5-Electric cable; 6-Pump; 7-Check valve; 8-Drainage pipe; 9-Support structure; 10-Manual gate valve; 11-Piezometer; 12-Pipeline pressure gauge; 13-Operation console; 14-Manometer; 15-Electromagnetic flowmeter; 16-Electric gate valve; 17-Return tank.

5. Experimental verification

The author of this article has built a temperature rise experimental platform for submersible motors, with the aim of measuring the actual temperature during the operation of the submersible motor. Fig. 11 shows a general view of the test platform. The key to the temperature rise experimental platform design was the installation of a 10 MPa manually adjustable gate valve at the submersible pump outlet to simulate the submersible electric pump discharge depth.

The working principle of the experimental platform is as follows: The submersible motor is connected with the submersible pump, which composition of submersible electric pump. The suction chamber is installed outside the submersible electric pump. The entire system is suspended in the experimental well through drainage pipelines and support structures. The manual gate valve is installed on the pipeline at the outlet of the submersible electric pump; the front of the manual gate valve is equipped with a manometer, which is used to control the outlet pressure of the submersible electric pump. Pressure gauge, flow meter, electromagnetic control valve, etc. are installed in the outlet pipe for measuring the flow of the submersible electric pump. When the test is carried out, the submersible electric pump outlet pressure is controlled by adjusting the opening of the manual gate valve, so as to achieve the regulation of the submersible electric pump operating conditions.

The author of this article installed four pressure sensors inside the submersible motor, two of which are located in the root of the teeth of the two parts of the stator of the submersible motor (A, B), another two are located in the pump (C, D),

(a) (b)

Fig. 12. Submersible pump (a) test process and (b) data recording.

Table 2
Comparison of pressure calculation results and the experimental pressure data

Number	Positions of pressure sensor	Test (MPa)	Calculated (MPa)	Error (%)
1	A	1.0828	1.1015	+1.698
2	B	1.0856	1.0965	+0.994
3	C	1.1124	1.1035	–0.806
4	D	1.0956	1.0924	–0.293

and the four pressure measuring elements are connected to the operation console on the ground for display of the pressure value at the measurement point. Fig. 12 shows the test process and data recording process of the submersible pump.

The pressure at the air gap inlet was tested at different flow rates. The comparison of the simulated calculation of pressure data with the experimental pressure data is shown in Table 2. It is not difficult to see through data comparison; the simulated calculation of pressure data agrees well with the experimental pressure data.

6. Conclusion

Based on CFD theory, this paper simulates the air gap flow field of submersible motor, and studies the influence of air gap inlet fluid flow on air gap fluid flow and air gap fluid pressure under different working conditions. The main conclusions are as follows:

(1) After the fluid enters the air gap of the motor, the speed increases rapidly due to the high-speed rotation of the rotor, and then reaches a relatively stable state. The maximum fluid velocity is located on the outer wall of the rotor, and the minimum fluid velocity is located on the inner wall of the motor stator.
(2) After the cooling water enters the air gap of the motor, the pressure shows a linear downward trend. The maximum pressure is located at the air gap inlet and the minimum pressure is located at the air gap outlet.
(3) The pressure drop at the inlet and outlet of the air gap fluid increases with the increase of the flow rate of the air gap inlet fluid, and the growth range decreases to different degrees.

The research results provide a basis for the design of submersible motor and the determination of fluid velocity in the motor.

Author contribution

Conceptualization, Shibin Zhang and Dingtang Zhang; methodology, Shibin Zhang; software, Shibin Zhang and Huayang Ren; validation, Shibin Zhang and Huyi Zhang; formal analysis, Shibin Zhang; investigation, Shibin Zhang and. Shuai Wang; writing-original draft preparation, Shibin Zhang, Yunbing Feng and Huayang Ren; writing-review and editing, Shibin Zhang, Rui Luo, Yunbing Feng and Huyi Zhang; All authors have read and agreed to the published version of the manuscript.

References

[1] Qianxun Industry Research, China Submersible Pump Industry Research Report, Qianxun Consuling Industry Research Center, Beijing, 2013.
[2] L. Zhang, Development of the submersible motor technology, PET Mach., 22 (1994) 48–49.
[3] L.H. Mo, X.Y. Zhu, T. Zhang, L. Quan, Y.Q. Wang, J. Huang, Temperature rise calculation of a flux-switching permanent-magnet double-rotor machine using electromagnetic-thermal coupling analysis, IEEE Trans. Magn., 54 (2018) 8201004, doi: 10.1109/TMAG.2017.2764182.
[4] Y.M. Xu, M.M. Ai, Y. Yang, Heat transfer characteristic research based on thermal network method in submersible motor, Int. Trans. Electr. Energy Syst., 28 (2018) e2507, doi: 10.1002/etep.2507.
[5] S.Y. Ding, G.H. Cui, Z.Y. Li, T.Y. Guan, Fluid and thermal performance analysis of PMSM used for driving, Heat Mass Transfer, 52 (2016) 571–579.
[6] K. Zhao, J. Luo, Performance comparison and analysis of different rotor structures of vehicle permanent magnet synchronous flat wire motor, Machines, 10 (2022) 212, doi: 10.3390/machines10030212.
[7] Q. Zhang, Z.-l. Li, X.-w. Dong, Y.-x. Liu, R. Yu, Comparative analysis of temperature field model and design of cooling

system structure parameters of submersible motor, J. Therm. Sci. Eng. Appl., 13 (2021) 051002 (16 Pages), doi: 10.1115/1.4049754.
[8] X.W. Zheng, Y.F. Wang, M. Jiang, S.B. Zhang, Numerical simulation of interior turbulent flow regulation of wet submersible motor, Wireless Pers. Commun., 102 (2018) 1443–1459.
[9] B.K. Guan, C. Di, Z. Ke, X.H. Bao, A numerical model for single-point bearing faults analysis in submersible induction motors, IEEJ Trans. Electr. Electron. Eng., 17 (2022) 1811–1819.
[10] Y.M. Xu, D.W. Meng, J. Tan, Research on design key technologies for high-power submersible motor, Adv. Mater. Res., 383–390 (2011) 414–419.
[11] D.G. Dorrell, Combined thermal and electromagnetic analysis of permanent-magnet and induction machines to aid calculation, IEEE Trans. Ind. Electron., 55 (2008) 3566–3582.
[12] A. Boglietti, A. Cavagnino, D. Staton, M. Shanel, M. Mueller, C. Mejuto, Evolution and modern approaches for thermal analysis of electrical machines, IEEE Trans. Ind. Electron., 56 (2009) 871–882.
[13] Y.Q. Wang, J. He, L. Ma, L. Wang, Y.Y. Sun, T. Wan, J.F. Dang, Research of the temperature field distribution based on FVM for oil-immersed transformer, Adv. Mater. Res., 1079–1080 (2014) 510–514.
[14] M.M. Ai, Y. Shan, The whole field temperature rise calculation of oil-immersed power transformer based on thermal network method, Int. J. Appl. Electromagn. Mech., 70 (2022) 55–72.
[15] J. Wang, L.H. Chen, Z.Y. Yu, Z.C. Wang, Y. Li, Design and analysis of a new cooling structure for interior permanent magnet synchronous motor with built-in fan, J. Phys. Conf. Ser., 2218 (2022) 012055, doi: 10.1088/1742-6596/2218/1/012055.
[16] N.Q. Shi, M. Wei, L.X. Zhang, X. Hu, B. Song, Design and research of cooling system for 2.5 MW permanent magnet wind turbine, Renewable Energy, 168 (2020) 97–106.
[17] S.X. Chen, S.Y. Ding, S.F. Shen, Y. Dai, Z. Yang, Analysis and suppression of electromagnetic vibrations in surface-mounted permanent magnet synchronous motors for ships, J. Electrical Eng. Technol., 38 (2023) 1275–1286+1298.
[18] M. Königs, H. Baccouche, S. Breser, T. Jöns, B. Löhlein, Simulation time reduction with 2.5D FEM analysis for axial flux machines, Power Electron. Drives, 8 (2023) 100–108.